Applied Ergonomics 80 (2019) 35–42

Contents lists available at ScienceDirect

Applied Ergonomics

journal homepage: www.elsevier.com/locate/apergo

Changes in under-shoe traction and fluid drainage for progressively worn shoe tread

Sarah L. Hemler[a], Danielle N. Charbonneau[a], Arian Iraqi[a], Mark S. Redfern[a], Joel M. Haight[b], Brian E. Moyer[c], Kurt E. Beschorner[a,*]

[a] Department of Bioengineering, University of Pittsburgh, 301 Schenley Place, 302 Benedum Hall, 3700 O'Hara Street, Pittsburgh, PA, 15261, USA
[b] Department of Industrial Engineering, University of Pittsburgh, 1025 Benedum Hall, 3700 O'Hara Street, Pittsburgh, PA, 15261, USA
[c] Mechanical Engineering Department, University of Pittsburgh – Johnstown, 225 Engineering & Science Building, 450 Schoolhouse Road, Johnstown, PA, 15904, USA

ARTICLE INFO

Keywords:
Biomechanics
Slips and falls
Available coefficient of friction

ABSTRACT

Shoe wear is known to increase slipping risk, but few studies have systematically studied this relationship. This study investigated the impact of progressive shoe wear on the available coefficient of friction (ACOF) and under-shoe fluid dynamics. Five different slip-resistant shoes were progressively worn using an accelerated, abrasive, wear protocol. The ACOF and fluid forces (the load supported by the fluid) were measured as shoes were slipped across a surface contaminated with a diluted glycerol solution. As the shoes became worn, an initial increase in ACOF was followed by a steady decrease. Low fluid forces were observed prior to wear followed by increased fluid forces as the worn region became larger. Results suggest that traction performance decreases particularly when the heel region without tread exceeds a size of 800 mm^2. This study supports the concept of developing shoe replacement guidelines based upon the size of the worn region to reduce occupational slips.

1. Introduction

Falls resulting from slipping are among the most common causes of non-fatal injuries in the workplace. In 2016, slips, trips, and falls were the second-leading cause for non-fatal occupational injuries accounting for 26.0% of all injuries (U.S. Department of Labor - Bureau of Labor Statistics, 2018). Of those incidents, over one-third caused workers to be away from work for 31 days or more and 28.3% of the incidences occurred in the service industry (U.S. Department of Labor - Bureau of Labor Statistics, 2018). Furthermore, 40–50% of fall-related injuries have been found to be attributed to slipping (Courtney et al., 2001). Thus, there is a need to develop prevention strategies for slips and falls.

Slips often occur when there is a reduction in friction between the shoe and floor, particularly when a liquid contaminant is present (Beschorner et al., 2014; Hanson et al., 1999). The friction that prevents slipping between the two surfaces is often measured using the available coefficient of friction (ACOF). A variety of tribometers have been used to measure ACOF (Aschan et al., 2005; Beschorner et al., 2007; Chang et al., 2001; Grönqvist, 1995; Singh and Beschorner, 2014). The required coefficient of friction (RCOF) represents friction required for walking (Redfern et al., 2001). A slipping incident is most likely to occur at the shoe-floor interface when the ACOF is less than the RCOF (Burnfield and Powers, 2006; Hanson et al., 1999).

Shoe outsole design is one important factor in friction analysis when liquid contaminants are present on the floor surface. Shoes marketed as slip-resistant (SR) tend to have tread patterns that have an increased ACOF compared to shoes not marketed as slip-resistant (Beschorner et al., 2017). A study conducted in the service industry showed that SR shoes can reduce the number of slip and falls by as much as 54% (Verma et al., 2011). However, variations in shoe design among SR shoes result in a broad range of ACOF values (Jones et al., 2018).

Variations in tread design (i.e. tread depth and width) have been shown to affect ACOF (Li and Chen, 2004; Li et al., 2006; Yamaguchi et al., 2017). Channels in shoe tread provide fluid dispersion pathways to reduce hydrodynamic pressures (Strandberg, 1985; Tisserand, 1985) and have been shown to reduce the risk of slipping compared to shoes without such channels (Beschorner et al., 2014). Hydrodynamic measurements have shown that under-shoe fluid pressure varies across the contact regions between the shoe sole and floor (Beschorner et al., 2014; Singh and Beschorner, 2014). Other research has shown increases in ACOF at modest wear levels and a reduction in ACOF for severely worn shoes in some cases (Grönqvist, 1995; Kim, 2000). Previous studies have shown that wear tends to be concentrated on the heel sections (Grönqvist, 1995). A recent review article suggested that accelerated

* Corresponding author.
E-mail addresses: slh148@pitt.edu (S.L. Hemler), dnc7@pitt.edu (D.N. Charbonneau), ari16@pitt.edu (A. Iraqi), mredfern@pitt.edu (M.S. Redfern), jhaight@pitt.edu (J.M. Haight), bmoyer@pitt.edu (B.E. Moyer), beschorn@pitt.edu (K.E. Beschorner).

https://doi.org/10.1016/j.apergo.2019.04.014
Received 24 August 2018; Received in revised form 12 February 2019; Accepted 26 April 2019
Available online 15 May 2019
0003-6870/

wear methodologies should be developed to shorten the observation time in order to assess shoes throughout their life (Chang et al., 2016). Thus, this study aims to detail changes in shoe traction and drainage across the shoe's life using an accelerated wear method to help guide shoe replacement criteria.

Replacement criteria for shoes have not been established. Previous research has shown that shoes worn for less than six months performed better than those worn for more than six months and that changing to a new pair of shoes had a 55% reduction in slip rate (Verma et al., 2014). However, just two states of wear were considered in that study (< 6 months old, > 6 months old). Furthermore, shoe age is an imprecise measure since it does not consider usage or environmental conditions that may influence wear rate. An alternative approach is to develop replacement thresholds using metrics based on the geometry of the worn shoe. This study tracked changes in the geometry of worn shoes to identify wear measures which were correlated to shoe performance changes.

The purpose of this study was to quantify changes in ACOF and under-shoe fluid loading as shoes were progressively worn using a simulated wear protocol. The secondary purpose was to determine a wear replacement threshold based on ACOF and fluid pressure measures.

2. Methods

A progression of wear-related changes in shoe traction performance was determined via iterations of mechanical testing, mold creation (to capture shoe tread geometry), and abrasion via a simulated wear protocol (Fig. 1A). During mechanical shoe testing, ACOF and under-shoe fluid pressures were measured as a robotic device moved the shoe across a contaminated surface (Fig. 1B). Molds of the heel tread geometry were generated using an apparatus that allowed the mold material to cure while the shoe was held in a fixed and consistent position (Fig. 1D). Shoes were progressively worn using an apparatus with a sliding abrasive belt and a means of adjusting the shoe angle (Hemler et al., 2017) (Fig. 1C).

2.1. Materials & procedures

2.1.1. Simulated wear protocol

The accelerated wear apparatus (Fig. 1C), consisting of a linear motion abrasion device (Ryobi BD4601; One World Technologies, Inc.; Anderson, SC, USA) and an angle-adjustable platform, was used to simulate wear of the right heel of the shoes (Hemler et al., 2017). The device slid abrasive paper (180 μm diameter particles) at 9.65 m/s across the heel with a normal force of 40 N, similar to abrasion resistance standards for footwear and previous research for abrasively removing shoe tread (Beschorner et al., 2014; ISO/IEC, 2001; Manning et al., 1990). A normal force lower than that produced during gait was used to reduce heat generation and due to an inability of the device to overcome friction forces when large normal forces were applied. One wear cycle consisted of abrading each shoe for 20 s at three angles (17° ± 1°, 7° ± 1°, and 2° ± 1°). The angles were chosen to simulate angles experienced from initial heel strike to flat foot (Kadaba et al., 1990). Each wear cycle was equivalent to a total sliding distance of 580 m (193 m at each angle). The angle of the shoe was defined relative to horizontal, which was the orientation of the shoe when it was placed on the floor without an applied external load. Each shoe was abraded until there were five wear cycles for which the fluid force was greater than 50 N (20% of the normal force; described in Section 2.2). Prior to each accelerated wear iteration, abrasive belt grease (Formax, No. F26) was applied to the abrasive paper to minimize increases in temperature between the shoe and the paper. After each wear cycle, residual grease was cleaned from the heel section of the tread using detergent and water, and then the heel section was rinsed with water and thoroughly dried.

Five pairs of shoes commonly worn in the service industry were included in the study and the right shoe for each pair was tested (Fig. 2). All shoes were claimed by their manufacturers to be 'slip-resistant' or 'anti-slip'. Detailed material compound was not available, but shoes were reported as having an outsole composed of 'rubber' or 'rubber compound'. Short-term hardness measurements were recorded at baseline using a Shore A durometer based on ASTM standard D2240 (ASTM, 2015) and the proportion of tread surface area to overall heel surface area, "tread proportion", was recorded (Table 1). To determine tread proportion, 3D models of the heel were created based on measurements of heel and tread geometry (ANSYS Design Modeler, ANSYS Inc., Canonsburg, Pennsylvania, USA). The software was then used to sum the areas on the contact surface of the tread as well as the areas in the tread channels that were parallel to the contact surface. The tread proportion was calculated as the ratio of the contact surface area to the total surface area (sum of contact area and tread channel area parallel to contact surface). The roughness of the continuous sections of each tread block was characterized by the maximum peak to valley height (R_z), which was averaged across five scans each using a sampling scan length of 1.6 mm and a cutoff frequency of 0.8 mm. Measurements were taken at five different locations on the shoe heels for the baseline tread and the fully worn region (i.e., "untreaded") at final wear using a 2D contact profilometer (Surtronic S-100, Taylor-Hobson, AMETEK, Leicester, England). Portions of this data set were included in a previous publication that compared a shoe wear model to experimental results (Moghaddam et al., 2019).

2.1.2. Mechanical testing of shoes

ACOF and fluid pressure measurements were conducted using a robotic slip tester (Fig. 1B). The slip tester included three electromagnet motors – one motor to control vertical displacement (Z-direction) and two horizontal motors to control horizontal movement (Y-direction) and foot angle, a force plate measuring shear and normal forces (vertical load capacity = 4450 N; BP400600−1K-Q2046, AMTI, Watertown, MA, 02472), and four fluid pressure sensors (Gems® 3100R10PG08F002) in a linear array in the X-direction of the device (Fig. 1B). A platform was mounted to the top of the force plate, which could be moved in the X-direction (medial-lateral); the platform and the force plate were fully constrained during testing procedures while the horizontal and vertical motors allowed for the shoe to translate in the Y and Z directions and rotate about the X-axis (3 degrees of freedom) (See Fig. 1B for axes of the testing device). The fluid pressure sensors, each with an inlet diameter of 3.2 mm, were installed in the top of this platform, spaced 25 mm apart. Forces and hydrodynamic pressures were recorded at 500 Hz. The device is conceptually similar to the Portable Slip Simulator device (Aschan et al., 2005; Iraqi et al., 2018a; Jones et al., 2018) but has 2 horizontal motors that can operate independently to permit active shoe-floor angle control (Fig. 1B).

Shoes were slid across a vinyl composite tile (Armstrong, 51804; R_a = 2.19 ± 0.29 μm, R_z = 16.13 ± 2.74 μm, R_q = 3.13 ± 0.42 μm) which was contaminated with a diluted glycerol solution (90% glycerol, 10% water by volume; 219 cP). Tile roughness was measured in three locations on the tile in four orientations, each 45° apart (sample length: 8 mm, cutoff length: 0.8 mm). Contaminant was spread across the tile prior to each test to ensure that the entire region interacting with the shoe was covered with contaminant. Measurements occurred using a shoe angle of 17° ± 1°, a speed of 0.3 m/s, and an average force of 250 N ± 10 N. These conditions were intended to approximate the angle (Albert et al., 2017; Iraqi et al., 2018a,b), speed (Albert et al., 2017; ASTM, 2011; Iraqi et al., 2018b), and normal force (Iraqi and Beschorner, 2017; Iraqi et al., 2018b) at the onset of slipping. These tests were performed at baseline (i.e., prior to any wear cycles) and after each wear cycle. ACOF data using this method has been demonstrated to predict slips (Iraqi et al., 2018a). Furthermore, as previous research has shown that fluid pressures may vary across the shoe surface (Beschorner et al., 2014; Singh and Beschorner, 2014), the slip tester platform was moved 5 mm in the X-direction four times for a total

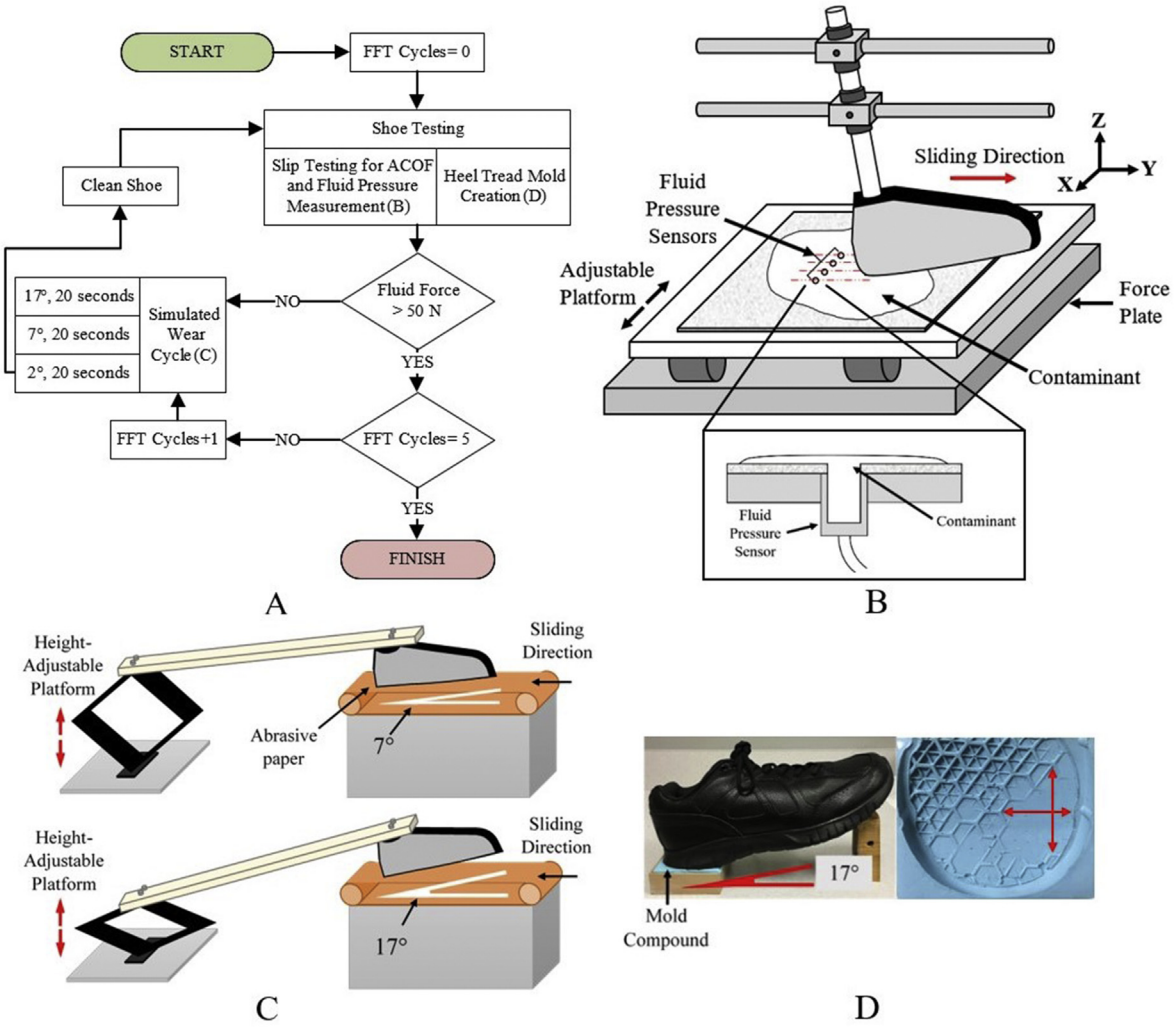

Fig. 1. A) Flowchart of mechanical testing and abrasive wear protocol. The Fluid Force Threshold (FFT) is described in Section 2.2. B) A robotic slip tester used to slide each shoe anteriorly across the contaminated tile along multiple parallel paths. Four fluid pressure sensors mounted above a force plate recorded fluid pressures and shear and normal forces, respectively. Cross-sectional view of contaminant and fluid pressure sensor is shown below the testing apparatus. C) Simulated wear apparatus on which the heel of each shoe was progressively worn at 17°, 7°, and 2°. Examples of wear at 17° and 7° are shown. D) Shoe heel placed in mold frame at 17° (left) and the length and width of the largest wear region indicated with red arrows on the heel tread mold (right). (For interpretation of the references to colour in this figure legend, the reader is referred to the Web version of this article.)

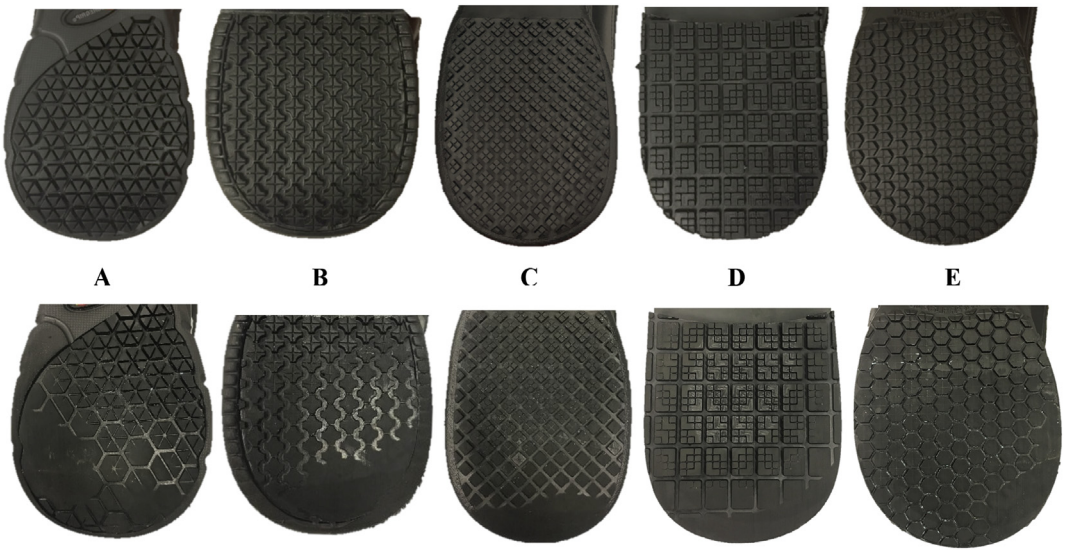

Fig. 2. The tread of the five slip-resistant shoes used in the study at baseline (top) and after all wear was completed (bottom).

Table 1
List of shoe code, brand, model, size, short-term hardness, baseline tread depth, initial contact area on the abrasion device at the three angles of wear, proportion of tread surface area to overall heel surface area, and heel edge type.

Shoe Code	Shoe Brand	Shoe Model	Shoe Size (US Men's)	Short Term Hardness (Shore A)	Baseline Tread Depth [mm]	Initial Contact Area [mm^2] (2°/7°/17°)	Tread Proportion	Heel Edge Type
A	Keuka	Galley 55014	9	56.4	3.7	249/180/145	0.48	Bevelled
B	safeTstep	Apollo 140060	8.5	63.5	2.7	191/118/91	0.32	Bevelled
C	Shoes for Crews	Falcon 6007	9	56.3	3.4	432/266/85	0.41	Square
D	SR Max	SRM 3500	9	50.1	2.8	271/147/44	0.57	Square
E	Tredsafe	M151044BU	9	60.5	2.4	264/325/160	0.66	Bevelled

of five trials and 20 pressure scans per measurement cycle.

2.1.3. Heel tread mold protocol

Heel tread at baseline and after each wear cycle was measured by creating a mold of the heel tread using a silicone rubber compound (Smooth-On Inc.; Macungie, PA; Oomoo® 25). To generate the mold, shoes were placed in a frame (92 mm × 76 mm x 28 mm), which was filled with the compound, at a sagittal plane angle of 17° (Fig. 1D). Prior to placement in the mold compound, shoe tread was lightly and uniformly coated with a spray petroleum-based oil (WD-40 Company; San Diego, CA, USA) to allow for easy removal of the shoe from the mold. The molds were used to determine the largest region of the heel that lacked any tread as wear progressed for each iteration. For iterations in which the entire heel had tread, the size of one lug from the tread pattern was measured as the largest region. Once a worn region developed, the size of the region without tread was characterized by the longest length (along the sliding axis) and width (perpendicular to sliding axis) uninterrupted by a tread block (Fig. 1D).

2.2. Data and statistical analysis

The average ACOF for each shoe, wear iteration, and angle was calculated starting 0.1 s before and ending 0.1 s after the shoe crossed the pressure sensors for a total of 0.2 s. ACOF for each frame was determined as the magnitude of the resultant shear force divided by the normal force (Eq. (1)) where F_{xi} and F_{y_i} are the shear forces and F_{zi} is the vertical ground reaction force for each frame (i). ACOF and fluid pressure data from two wear cycles and select trials were excluded because the normal force was outside of the desired range (240–260 N). Experimental complications also caused data from one shoe for one wear cycle to be excluded.

$$\mu_i = \frac{\sqrt{{F_{xi}}^2 + {F_{y_i}}^2}}{F_{zi}} \quad (1)$$

The peak fluid pressure was recorded and the force supported by the fluid (fluid force) across the shoe was calculated for each wear cycle. Fluid pressures above five standard deviations from the baseline pressure levels were included in the measurements (Beschorner et al., 2014). The fluid force was determined using numerical integration (Eq. (2)), where p_i is the fluid pressure at the ith frame, Δx is the distance between scans in the direction perpendicular to sliding (5 mm), v is the sliding velocity (0.3 m/s), and Δt is the time between each frame (0.002 s) (Singh and Beschorner, 2014). The fluid force was thus summed for all fluid pressure readings across the five trials. Fluid forces were also categorized by percent of normal force during mechanical shoe testing (< 25 N or < 10%; 25–50 N or 10–20%; > 50 N or > 20%). Each shoe was worn until there were five wear cycles – indicated as Fluid Force Threshold (FFT) cycles – for which the fluid force was greater than 50 N (Fig. 1A).

$$F_{fluid} = \sum p_i \, \Delta x \, \Delta y = \sum p_i \, \Delta x \, v \, \Delta t \quad (2)$$

Statistical analyses were performed to determine the relationships between ACOF, fluid force (continuous and categorical), the region without tread, tread proportion, and the sliding distance between and within each shoe type. Three generalized linear regression models were used to determine the relationships of each of the dependent variables – ACOF, fluid force, and region without tread – with the independent variables – shoe type (categorical), sliding distance (continuous) as shoes were worn, and their interaction. In the model, a square root transformation was used for fluid force to achieve normally-distributed residuals. Furthermore, a generalized linear regression model was used to determine ACOF differences across fluid force categories and shoe type. Specifically, ACOF was the dependent variable and the independent variables were the fluid force category, shoe type, and their interaction. If an interaction effect was observed between the fluid force category and shoe type, then a Tukey's HSD test was performed to determine significance between the three fluid force categories within each shoe type. Only comparisons across fluid force category within each shoe were analyzed in order to reduce the number of comparisons and maintain sufficient power.

3. Results

ACOF values ranged from 0.057 to 0.406 with a mean ACOF of 0.189. The mean of the standard deviation across a set of ACOF trials within a wear cycle was 0.007 with a maximum standard deviation of 0.025. ACOF increased after the first wear cycle for Shoes A, B, C, and E followed by steady decrease across wear cycles (Fig. 3). For Shoe D, an initial ACOF decrease of 0.097 occurred after the first wear cycle followed by a continued steady decrease. ACOF values when a fluid force first exceeded 50 N were 27%–50% lower than their initial values and 37%–63% lower than the peak values (Table 2). The regression analysis showed that ACOF was affected by the shoe type ($p < 0.001$), the sliding distance ($p < 0.001$), and their interaction ($p < 0.001$).

Fluid force values ranged from 0 to 97 N. During the initial wear

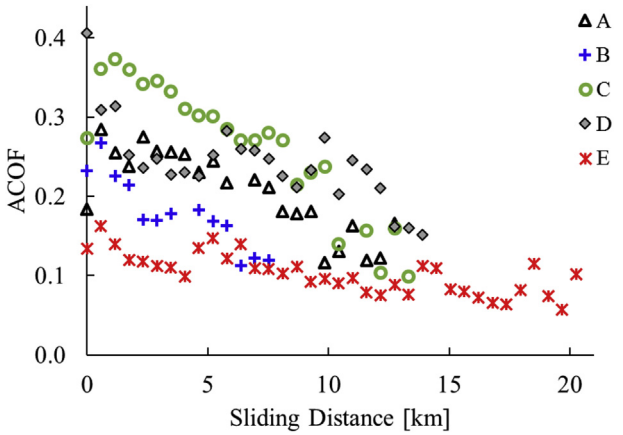

Fig. 3. ACOF values plotted against the sliding distance that each shoe was worn on the abrasion device. A sliding distance of 0 represents baseline (prior to wear).

Table 2
Baseline (no wear), maximum, and minimum ACOF values across wear cycles, the ACOF values when the fluid force initially reached 50N, and roughness measurements (R_z) of the tread at baseline (no wear) and of the untreaded region at final wear.

Shoe Code	Total Sliding Distance [km]	Baseline ACOF	Maximum ACOF	Minimum ACOF	ACOF when fluid force first exceeded 50 N	R_z [μm]	
						Baseline	Final
A	12.7	0.183	0.284	0.117	0.117	15.60	13.50
B	7.5	0.232	0.267	0.112	0.168	19.10	14.50
C	13.3	0.269	0.366	0.099	0.136	11.40	14.67
D	13.9	0.406	0.406	0.151	0.202	7.25	12.90
E	20.3	0.134	0.163	0.057	0.066	15.25	12.80

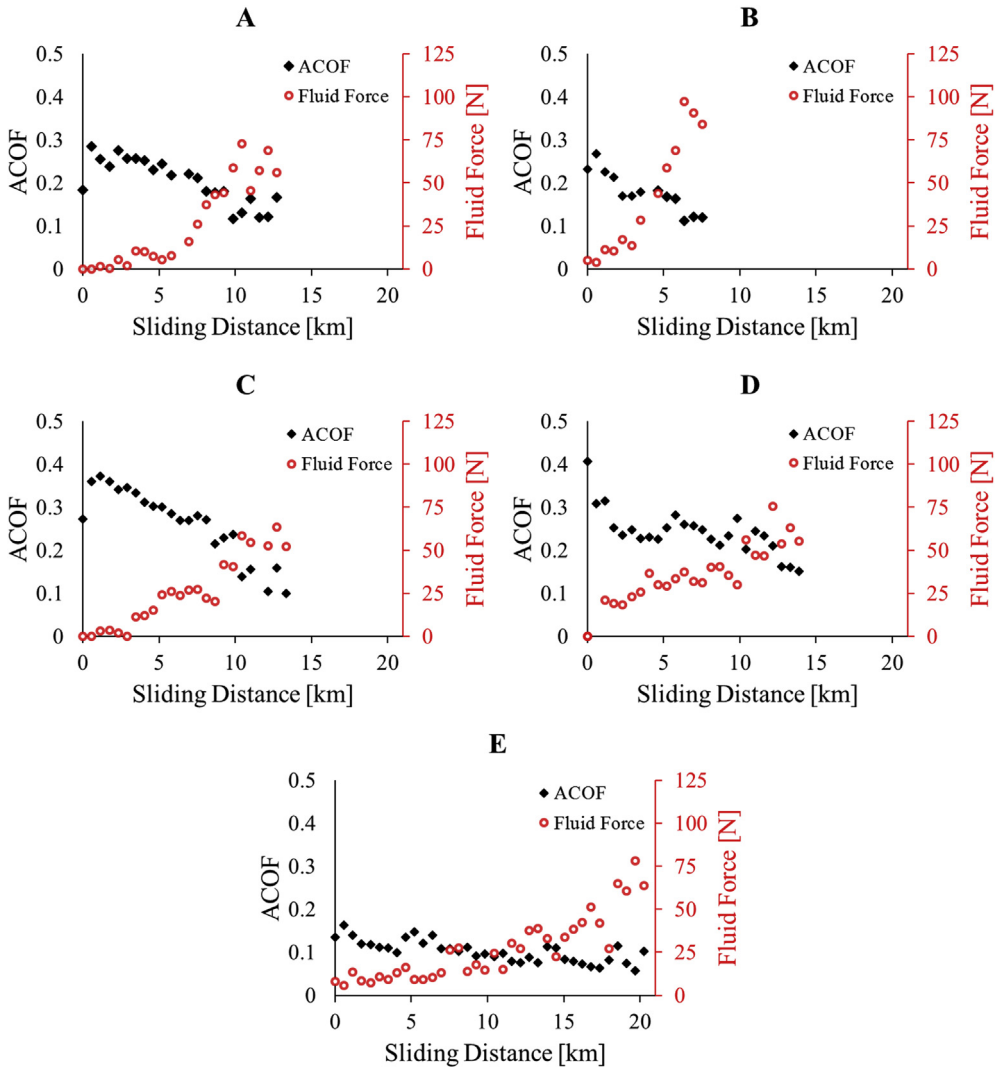

Fig. 4. Fluid force and ACOF plotted against the sliding distance that each shoe was worn on the abrasion device. A sliding distance of 0 represents baseline (prior to wear).

cycles, when most ACOF values increased relative to baseline, fluid pressures were under 25 N (Fig. 4). For shoes A, B, and C, there was a distinct increase of fluid force between 4 and 8 km of wear distance accompanied by a steady decrease of ACOF. Shoe D showed an early increase in fluid force (1.2 km of wear), which was also accompanied by a steady decrease of ACOF. Shoe E showed a steady increase in fluid force across all wear cycles. Fluid force was affected by the shoe type ($p < 0.001$), the sliding distance ($p < 0.001$), and the interaction between shoe type and sliding distance ($p < 0.001$).

Regions of the heel with fully worn tread developed on the lateral side of the heel for shoe A and the medial side of the heel for shoes B, C, D, and E (Fig. 2). Within the untreaded region, the length parallel to the sliding axis was greater than the length perpendicular to the sliding axis for shoe A, but smaller for shoes B, C, D, and E. These regions of the untreaded region ranged from 7 mm^2 to 26 mm^2 at baseline and 1192 mm^2 to 1954 mm^2 after the final wear cycle (Fig. 5). The region without tread when the fluid force first exceeded 50 N ranged from 840 mm^2 to 1730 mm^2 (mean: 1300 mm^2; standard deviation: 320 mm^2). Subsequently, this region grew at varying rates for each shoe. The region without tread for shoe B and shoe E increased the fastest and slowest, respectively. This region was affected by the shoe type ($p < 0.001$), the sliding distance ($p < 0.001$), and the interaction

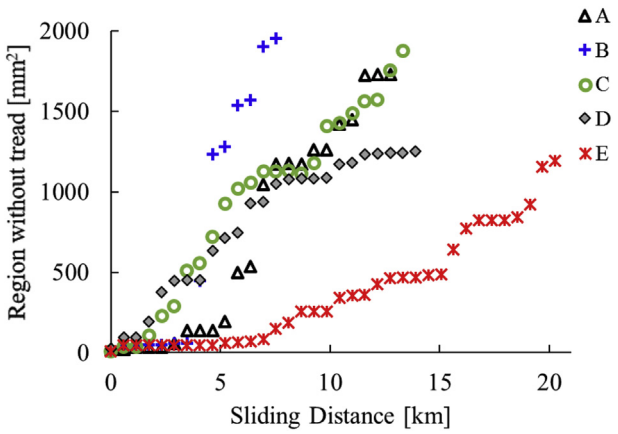

Fig. 5. Region without tread (measured at each wear iteration) plotted against wear distance across the wear device.

between shoe type and sliding distance ($p < 0.001$) (Fig. 5).

Increased fluid loading was associated with a reduction in ACOF which was affected by shoe type ($p < 0.001$), fluid force category ($p < 0.001$), and their interaction ($p < 0.001$) (Fig. 6). Significant decreases in ACOF between all fluid force categories occurred for two shoes (C and D) and ACOF significantly decreased between at least two categories for all shoes. The largest decreases in mean ACOF per category were observed in the shoes with the largest ACOF values at baseline (C and D) (Fig. 6).

4. Discussion

The results confirm that shoe slip-resistance changes as the tread wears. An increase in ACOF and relatively unchanged fluid forces accompanied the initial wear process (< 3 km wear distance) for four of the shoes. After reaching the peak ACOF, fluid forces increased while ACOF values decreased for all shoes. Sudden increases in fluid force occurred at wear distances between 1 and 11 km for four of the shoes indicating that wear thresholds may exist where the shoe performance suddenly changes. The amount of ACOF decrease appeared to scale with the magnitude of the baseline ACOF: the shoes with the highest baseline ACOF tended to have the largest decrease in ACOF among the fluid force categories.

The results were generally consistent with the literature. Slightly worn shoes tended to have an increase in ACOF consistent with Grönqvist (1995) who suggested this may be due to an optimum combination of surface roughening and sufficient tread depth. In contrast to Grönqvist's suggestions, there was not a clear effect of the change in surface roughness on ACOF for these shoes. An alternative explanation is that slightly worn shoes may lead to higher ACOF due to an increase in contact area as the geometry of the shoe conforms to the floor surface (Moghaddam, 2018; Moghaddam et al., 2019; Moghaddam et al., 2014). For all shoes, a decrease in ACOF occurred for severe wear, which aligns with previous research findings that highly worn shoes are associated with a higher risk of slipping (Grönqvist, 1995; Verma et al., 2014). Furthermore, this study supports previous research that related higher fluid forces with increased slip risk and lower ACOF (Beschorner et al., 2014; Beschorner et al., 2009).

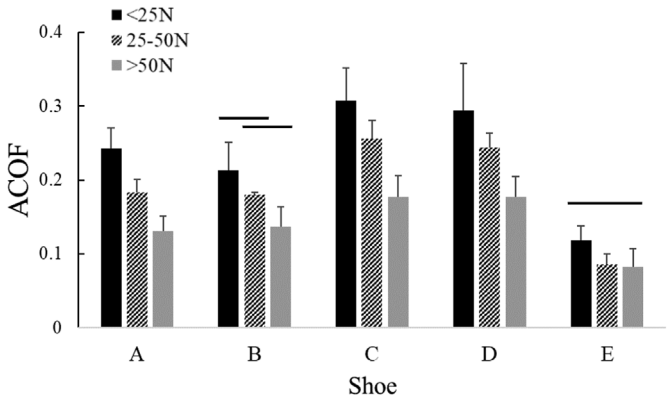

Fig. 6. Mean ACOF for each fluid force category (< 25 N, 25–50 N, and > 50 N). Error bars represent standard deviations within fluid force categories. Categories within each shoe connected by a bar are not significantly different.

Prior to the sudden increase in fluid force, there was gradual decrease in ACOF. This behavior may be due to the shape factor of the tread which is defined by the loaded area of a rubber block divided by its area of lateral surface that is free to expand (Imbimbo and De Luca, 1998). The reduction of tread depth will increase the shape factor of a tread block by decreasing the area of the lateral surface that is free to expand. Consequently, this may result in lower deformability (Imbimbo and De Luca, 1998) of the tread block. In tire traction applications, the geometry of the tire tread block (given the same volumetric properties and contact area) in contact with a rigid surface affects rubber deformation (Sridharan and Sivaramakrishnan, 2012). On the other hand, tread blocks that have too much height (and subsequently tread channels that are too deep) can reduce the ACOF (Maegawa et al., 2016; Yamaguchi et al., 2017). Specifically, previous research showed that a large tread depth could lead to lower bending stiffness, which could result in an increase in deflection during sliding. This increase in deflection can reduce the contact area and subsequently decrease the friction force in boundary lubrication. Thus, this research suggests there may be an optimal tread depth that minimizes hydrodynamic pressures, reduces the shape factor, and has a sufficiently high bending stiffness.

Although ACOF decreased as the shoes were worn, increased fluid forces were more dependent on the size of the region without tread (Fig. 5). Faster growth in the untreaded region (e.g. Shoe B) was also associated with faster onset of high fluid pressures, whereas a slower growth in untreaded region (e.g. Shoe E) was associated with slower onset of high fluid pressures. Currently, some footwear providers offer tread gauge meters for tracking the utility of worn shoes (ShoesForCrews, 2019). However, this metric may not capture the salient features of the worn shoe condition. The minimum tread depth reached 0 mm as soon as the untreaded region began forming which occurs early in the wear process (Fig. 7). Furthermore, the reduction of the minimum tread depth to 0 mm occurred prior to substantial increases in the fluid forces. Specifically, this change occurred prior to fluid forces equal to 10% of the normal load during testing (25N) for all shoe types. Thus, the size of the region without tread may be more relevant to the under-shoe tribology dynamics.

Tread may start to be too worn when under-shoe fluid forces rise above 10% of the vertical load (25 N), acting as a first indicator of replacement (Fig. 6). A fluid force greater than 20% of the vertical load (50 N) may serve as a replacement threshold since our findings suggest that an ACOF decrease of 25%–50% of the baseline value may be associated with these fluid forces. Fluid forces exceeded this level when the region without tread exceeded between 840 mm^2 and 1720 mm^2. A conservative estimate might be to replace shoes at the lower limit of this range (approximately 800 mm^2). This information has potential to be used to guide footwear replacement thresholds.

While this study was not designed to determine the tread design parameters that influenced wear progression, notable differences were observed across the footwear designs. For example, Shoe B wore out in the shortest sliding distance whereas Shoe E wore out over the longest distance. The statistical modeling in this study using a nominal code for shoe type has limited predictive ability when extrapolating to other tread patterns and materials. However, a post-hoc analysis was performed to further explore the differences across shoes. Interestingly, the difference in the rate of response to wear might be explained by the

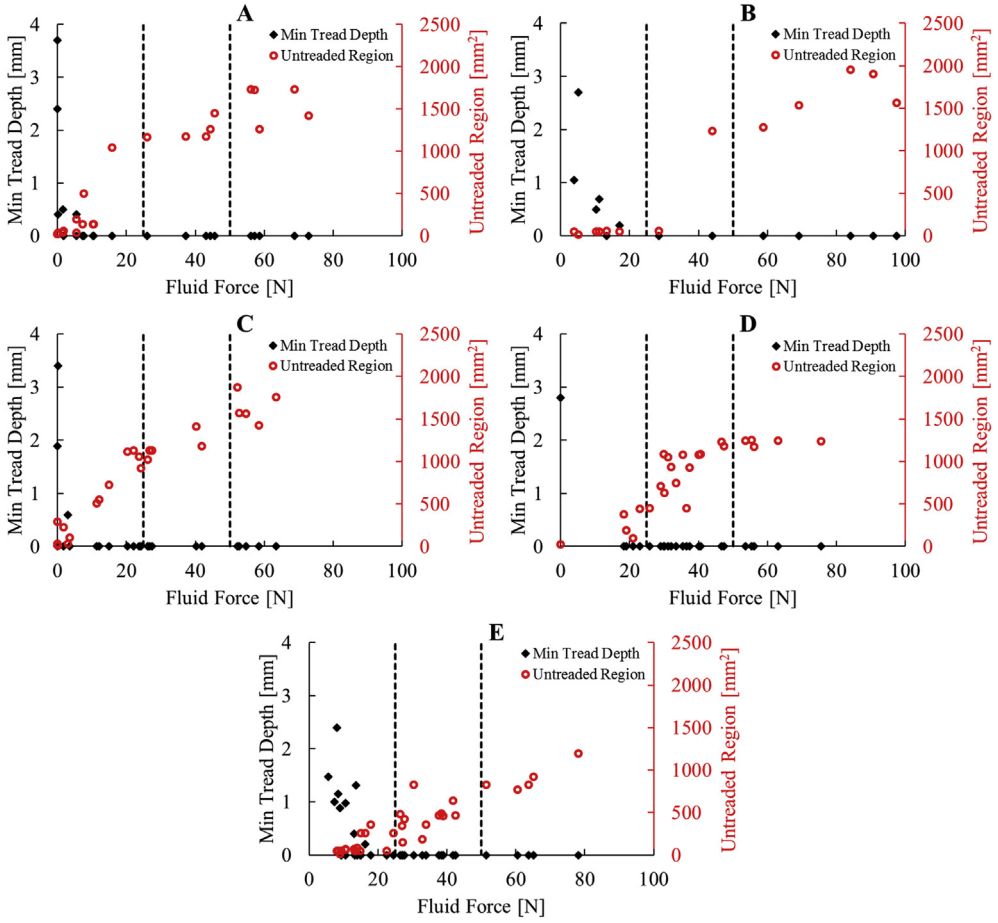

Fig. 7. Minimum tread depth and the size of the untreaded region plotted against fluid force for each shoe. Fluid force thresholds of 25N and 50 N are indicated with vertical dashed lines. Minimum tread depth reached 0 when the untreaded region began forming.

proportion of the heel's surface covered in tread (Table 1). A bivariate correlation analysis was used to determine the relationship between tread proportion and total wear distance until the shoe completed the protocol. Increased tread proportion was associated with an increased number of wear cycles and thus, increased total sliding distance ($p = 0.026$). As such, Shoe E had the largest proportion of tread coverage over the heel (tread proportion). This effect may be associated with Archard's law which describes how the wear rate is proportional to the contact pressure (Archard, 1953; Moghaddam et al., 2019). Thus, a larger tread proportion produces a larger contact area and reduces the contact pressure on the individual tread blocks. However, a more robust study with more shoes and systematically varied tread coverage would need to be conducted to confirm this relationship.

As this is the first research study to examine the association between progressive shoe wear and ACOF, fluid force, and region without tread, certain limitations should be acknowledged. First, only a limited number of shoes were examined, chosen as industry-marketed slip-resistant shoes. These shoes have significant tread to provide fluid drainage. Other types of shoes may behave differently. Second, the wear device was effective in producing rapid wear that had profiles on the heel similar in appearance to actual wear from walking. However, there may be unforeseen differences between these methods and naturally worn shoes due to varied gait biomechanics. Furthermore, extending this research to additional flooring (e.g., roughness, hardness) and contaminants with varying material properties (e.g. viscosity, surface tension) might lead to different wear thresholds. Improvements for future use of this simulated wear protocol could include employing personal gait characteristics (supination/protonation, heel strike angle, etc.) to better approximate natural wear.

These results suggest that a worn region on the heel with a size larger than 800 mm^2 leads to increased fluid forces and a reduction in ACOF. Research has shown that these changes are consistent with an increase in slip risk (Beschorner et al., 2014; Hanson et al., 1999). Thus, the amount of wear in specific areas on the shoe may be useful in determining a threshold for shoe replacement to prevent slips. The results are promising and useful for the development of future guidelines for shoe evaluation and for further research taking into account the material properties of shoe wear and flooring and also the gait biomechanics.

Funding

This study was funded by a grant from the National Institute for Occupational Safety and Health (NIOSH R01OH010940), the National Institute of Arthritis and Musculoskeletal and Skin Diseases (R43AR064111), and the National Science Foundation Graduate Research Fellowship Program (NSF 16-104).

Appendix A. Supplementary data

Supplementary data to this article can be found online at https://doi.org/10.1016/j.apergo.2019.04.014.

References

Albert, D.L., Moyer, B.E., Beschorner, K.E., 2017. Three-dimensional shoe kinematics during unexpected slips: implications for shoe–floor friction testing. IISE Trans. Occup. Ergon. Hum. Factors 5 (1), 1–11.
Archard, J., 1953. Contact and rubbing of flat surfaces. J. Appl. Phys. 24 (8), 981–988.

Aschan, C., Hirvonen, M., Mannelin, T., Rajamäki, E., 2005. Development and validation of a novel portable slip simulator. Appl. Ergon. 36 (5), 585–593.
ASTM, American Society for Testing and Materials, 2011. ASTM F2913-11: Standard Test Method for Measuring the Coefficient of Friction for Evaluation of Slip Performance of Footwear and Test Surfaces/Flooring Using a Whole Shoe Tester. ASTM International, West Conshohocken, PA.
ASTM, American Society for Testing and Materials, 2015. ASTM D2240-15: Standard Test Method for Rubber Property-Durometer Hardness. ASTM International.
Beschorner, K.E., Albert, D.L., Chambers, A.J., Redfern, M.S., 2014. Fluid pressures at the shoe–floor–contaminant interface during slips: effects of tread & implications on slip severity. J. Biomech. 47 (2), 458–463.
Beschorner, K.E., Jones, T.G., Iraqi, A., 2017. The combined benefits of slip-resistant shoes and high traction flooring on coefficient of friction exceeds their individual contributions. In: Paper Presented at the Proceedings of the Human Factors and Ergonomics Society Annual Meeting.
Beschorner, K.E., Lovell, M., Higgs III, C.F., Redfern, M.S., 2009. Modeling mixed-lubrication of a shoe-floor interface applied to a pin-on-disk apparatus. Tribol. Trans. 52 (4), 560–568.
Beschorner, K.E., Redfern, M.S., Porter, W.L., Debski, R.E., 2007. Effects of slip testing parameters on measured coefficient of friction. Appl. Ergon. 38 (6), 773–780.
Burnfield, J.M., Powers, C.M., 2006. Prediction of slips: an evaluation of utilized coefficient of friction and available slip resistance. Ergonomics 49 (10), 982–995.
Chang, W.-R., Grönqvist, R., Leclercq, S., Brungraber, R.J., Mattke, U., Strandberg, L., et al., 2001. The role of friction in the measurement of slipperiness, Part 2: survey of friction measurement devices. Ergonomics 44 (13), 1233–1261.
Chang, W.-R., Leclercq, S., Lockhart, T.E., Haslam, R., 2016. State of science: occupational slips, trips and falls on the same level. Ergonomics 59 (7), 861–883.
Courtney, T.K., Sorock, G.S., Manning, D.P., Collins, J.W., Holbein-Jenny, M.A., 2001. Occupational slip, trip, and fall-related injuries–can the contribution of slipperiness be isolated? Ergonomics 44 (13), 1118–1137.
Grönqvist, R., 1995. Mechanisms of friction and assessment of slip resistance of new and used footwear soles on contaminated floors. Ergonomics 38 (2), 224–241.
Hanson, J.P., Redfern, M.S., Mazumdar, M., 1999. Predicting slips and falls considering required and available friction. Ergonomics 42 (12), 1619–1633.
Hemler, S.L., Charbonneau, D.N., Beschorner, K.E., 2017. Effects of shoe wear on slipping–implications for shoe replacement threshold. In: Paper Presented at the Proceedings of the Human Factors and Ergonomics Society Annual Meeting.
Imbimbo, M., De Luca, A., 1998. FE stress analysis of rubber bearings under axial loads. Comput. Struct. 68 (1), 31–39.
Iraqi, A., Beschorner, K.E., 2017. Vertical ground reaction forces during unexpected human slips. In: Paper Presented at the Proceedings of the Human Factors and Ergonomics Society Annual Meeting.
Iraqi, A., Cham, R., Redfern, M.S., Beschorner, K.E., 2018a. Coefficient of friction testing parameters influence the prediction of human slips. Appl. Ergon. 70, 118–126.
Iraqi, A., Cham, R., Redfern, M.S., Vidic, N.S., Beschorner, K.E., 2018b. Kinematics and kinetics of the shoe during human slips. J. Biomech. 74, 57–63.
ISO/IEC, 2001. ISO 20871:2001 Footwear - Test Methods for Outsoles - Abrasion Resistance. ISO/IEC, Geneva, Switzerland.
Jones, T., Iraqi, A., Beschorner, K.E., 2018. Performance testing of work shoes labeled as slip resistant. Appl. Ergon. 68, 304–312.
Kadaba, M.P., Ramakrishnan, H., Wootten, M., 1990. Measurement of lower extremity kinematics during level walking. J. Orthop. Res. 8 (3), 383–392.
Kim, I.-J., 2000. Wear progression of shoe heels during slip resistance measurements. In: Paper Presented at the Proceedings of the Human Factors and Ergonomics Society Annual Meeting.
Li, K.W., Chen, C.J., 2004. The effect of shoe soling tread groove width on the coefficient of friction with different sole materials, floors, and contaminants. Appl. Ergon. 35 (6), 499–507.
Li, K.W., Wu, H.H., Lin, Y.-C., 2006. The effect of shoe sole tread groove depth on the friction coefficient with different tread groove widths, floors and contaminants. Appl. Ergon. 37 (6), 743–748.
Maegawa, S., Itoigawa, F., Nakamura, T., 2016. A role of friction-induced torque in sliding friction of rubber materials. Tribol. Int. 93, 182–189.
Manning, D., Jones, C., Bruce, M., 1990. Proof of shoe slip-resistance by a walking traction test. J. Occup. Accid. 12 (4), 255–270.
Moghaddam, S.R.M., 2018. Computational Models for Predicting Shoe Friction and Wear. (Doctor of Philosophy). University of Pittsburgh.
Moghaddam, S.R.M., Hemler, S.L., Redfern, M.S., Jacobs, T.D., Beschorner, K.E., 2019. Computational Model of Shoe Wear Progression. Accepted for publication to Wear.
Moghaddam, S.R.M., Iraqi, A., Beschorner, K.E., 2014. Finite element model of wear progression in shoe soles. In: Paper Presented at the STLE Tribology Frontiers Conference, Chicago.
Redfern, M.S., Cham, R., Gielo-Perczak, K., Grönqvist, R., Hirvonen, M., Lanshammar, H., et al., 2001. Biomechanics of slips. Ergonomics 44 (13), 1138–1166.
ShoesForCrews, 2019. Shoe care and cleaning tips. Retrieved from https://www.shoesforcrews.com/sfc3/index.cfm?changeWebsite=US_en&route=inserts.QA/cleaning_caring , Accessed date: 18 January 2019.
Singh, G., Beschorner, K.E., 2014. A method for measuring fluid pressures in the shoe–-floor–fluid interface: application to shoe tread evaluation. IIE Trans. Occup. Ergon. Hum. Factors 2 (2), 53–59.
Sridharan, K., Sivaramakrishnan, R., 2012. Dynamic behavior of tyre tread block. Am. J. Eng. Appl. Sci. 5 (2).
Strandberg, L., 1985. The effect of conditions underfoot on falling and overexertion accidents. Ergonomics 28 (1), 131–147.
Tisserand, M., 1985. Progress in the prevention of falls caused by slipping. Ergonomics 28 (7), 1027–1042.
U.S. Department of Labor - Bureau of Labor Statistics, 2018. Nonfatal Occupational Injuries and Illnesses Requiring Days Away from Work, 2016. Retrieved from, Washington, D.C.
Verma, S.K., Chang, W.R., Courtney, T.K., Lombardi, D.A., Huang, Y.-H., Brennan, M.J., et al., 2011. A prospective study of floor surface, shoes, floor cleaning and slipping in US limited-service restaurant workers. Occup. Environ. Med. 68 (4), 279–285.
Verma, S.K., Zhao, Z., Courtney, T.K., Chang, W.-R., Lombardi, D.A., Huang, Y.-H., et al., 2014. Duration of slip-resistant shoe usage and the rate of slipping in limited-service restaurants: results from a prospective and crossover study. Ergonomics 57 (12), 1919–1926.
Yamaguchi, T., Katsurashima, Y., Hokkirigawa, K., 2017. Effect of rubber block height and orientation on the coefficients of friction against smooth steel surface lubricated with glycerol solution. Tribol. Int. 110, 96–102.